Front. Optoelectron. China 2008, 1(3–4): 279–284
DOI 10.1007/s12200-008-0057-6

RESEARCH ARTICLE

A portable functional imaging instrument for psychology research based on near-infrared spectroscopy

Xiaohua LV, Yi ZHENG, Ting LI, Zhongxing ZHANG, Hui GONG (✉)

The Key Laboratory of Biomedical Photonics of Ministry of Education, Wuhan National Laboratory for Optoelectronics, Huazhong University of Science and Technology, Wuhan 430074, China

Abstract To aid psychology researches on the function of the prefrontal cortex, a 16-channel brain functional imaging instrument based on near-infrared spectroscopy is developed. The probe of the instrument, covering a detection area of 15 cm × 4.4 cm of the prefrontal cortex, is made flexible and is easy to fix to the forehead. By employing multi-wavelength LEDs as light sources, using integrated detectors and choosing a USB-interface-based data acquisition device, the whole system is portable and convenient to use, which is good for psychological experiments. The system software is developed using Visual C++ 6.0, which controls the imaging process, measurement data plotting and storage. The maximal temporal resolution is about 100 ms. Noise and long-term drift test are given. The Valsalva maneuver experiment is used to validate the reliability of the instrument for monitoring hemodynamic changes.

Keywords near-infrared spectroscopy, temporal resolution, functional brain activity, prefrontal cortex

1 Introduction

The importance of psychology as a way for understanding the mechanisms underlying human behavior is well recognized. Mapping brain activity is important for psychological research. Techniques such as electroencephalography (EEG) [1], functional Magnetic Resonance Imaging (fMRI) [2,3] and Positron Emission Tomography (PET) have been widely used in the field. These techniques, although powerful, are very expensive and not easy to use. In most cases, the subjects are constrained in a limited space during experiments, which will have unwanted effects on the response of the subjects.

Translated and revised from *Chinese Journal of Biomedical Engineering*, 2007, 26(6): 898–902 [译自: 中国生物医学工程学报]

E-mail: huigong@mail.hust.edu.cn

Near-infrared spectroscopy (NIRS) is a relatively new technique for functional brain imaging [4,5] and if appropriately designed, it is easy to use and allows the subject to behave more naturally during experiments. NIRS is an optical method which uses near-infrared light as the probing light to get relatively large penetration depth. It can be used to detect non-invasively the relative change of the concentration of oxy- and deoxy-hemoglobin [6] in regions in the brain activated by behavioral stimulation. Various systems based on NIRS have been reported. There are three main types of the NIRS system [7–9] — time-resolved systems, frequency-domain systems and continuous-wave systems. Time-resolved systems require the use of a pulsed light source, while frequency-domain systems require high frequency modulation of the light source. None of these types are relatively complex and are suitable for psychological research in natural situations. Only continuous-wave (CW) type NIRS systems use a continuous-wave light source and have the potential to be portable and easy to use.

In this paper, a CW type NIRS functional imaging instrument that is suitable for psychological researches on the function of the prefrontal cortex is described. The components have been carefully selected for the purposes of portability and ease of use, and a certain software has been developed to simplify the experiment process. The probe is specifically designed for easy mounting, comfortable to wear and assures the penetration depth of the probing light. Experiments to evaluate the new instrument are also presented.

2 Theory

Local brain activity, associated with increase in oxygen consumption, is accompanied by changes in local cerebral blood volume (CBV) and cerebral blood flow (CBF), which is termed neurovascular coupling [10]. Activities of brain cells are associated with an increase of oxygen

consumption. The initial increase in oxygen supply by CBF exceeds the increased oxygen consumption, which leads to increase in intravascular hemoglobin oxygenation during brain activity. Oxygenated and deoxygenated hemoglobin (HbO_2 and Hb) are the main absorption chromophores [11] in the brain within the near-infrared light range (700–900 nm), and the absorption spectra of the two have different characteristics. Therefore, based on light absorption measurements, concentration changes of these molecules can be measured during brain activation.

Optical density (OD) determines the attenuation of light while it propagates through a tissue. The optical density change (ΔI_{OD}) parallels the hemoglobin concentration change if the overall absorption change is small. Consequently, the relationships can be expressed as follows:

$$\Delta I_{OD(850)} = k\Delta[HbO_2] + k'\Delta[Hb], \quad (1)$$

$$\Delta I_{OD(735)} = t\Delta[HbO_2] + t'\Delta[Hb], \quad (2)$$

where $\Delta I_{OD(850)}$ and $\Delta I_{OD(735)}$ indicate optical density changes at 850 and 735 nm wavelengths, $\Delta[HbO_2]$ and $\Delta[Hb]$ denote the concentration changes of HbO_2 and Hb, respectively. k, k', t, and t' are determined by the absorption coefficient and the average optical path, whose numerical values can be obtained from measurements on model systems [12]. Using this method, we get the equations describing the relationship between hemodynamic parameters and ΔI_{OD}:

$$\Delta[HbO_2] = \Delta I_{OD(850)} - 0.5643\Delta I_{OD(735)}, \quad (3)$$

$$\Delta[Hb] = 0.7538\Delta I_{OD(735)} - 0.4341\Delta I_{OD(850)}, \quad (4)$$

$$\Delta[HbT] = \Delta[Hb] + \Delta[HbO_2] = 0.5659\Delta I_{OD(850)} + 0.1895\Delta I_{OD(735)}. \quad (5)$$

$\Delta[HbT]$ in Eq. (5) denotes the change of CBV. Using a backscattering configuration, the functional imaging system can supply information about ΔI_{OD}, and the concentration changes of HbO_2, Hb and CBV (HbT) of the detected brain region can then be calculated using the formulae above.

3 Instrument design

As shown in Fig. 1, the system consists of four main parts: the imaging probe (including sources and detectors), the control box (including power supply, LED drivers, signal filters and amplifiers), the USB data acquisition device and a laptop computer. The whole system is under the control of the software running on the computer. The light source in the probe is injected near infrared photons into the brain and the back scattering photons exit in the brain and are detected in the probe. The detected signal is acquired by using a USB data acquisition device and transferred into the computer, where the data is analyzed and the results that reflect the brain activity are displayed on the screen.

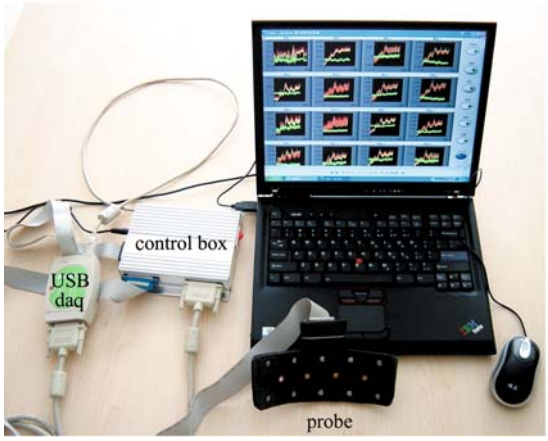

Fig. 1 Photograph of the whole system

3.1 Probe design

The probe is the key unit in the whole system. The light sources and detectors are chosen considering the requirement of portability. The probe is also designed for flexibility, so that it can be easily mounted and maintain good contact with the forehead.

3.1.1 Light sources

The light source must have a narrow spectral width so that spectroscopy can be conducted. Because the CW type NIRS system is an intensity measurement based system, the light source needs to have sufficient intensity to give a high signal-to-noise ratio.

LED is chosen as the light source for the system [13]. LED can be made small and light-weight with negligible heat problems, so that it can be directly embedded in the probe without the need of light-coupling via optical fibres. A type of three-wavelength near-infrared LED (L4X735/4X805/4X850-40Q96-I, Epitex, Japan) is used in the functional imaging instrument. The LED encapsulates three types of LED chips in one package, the output wavelength of each type centers respectively at 735, 805 and 850 nm with a spectral width of about 40 nm. As stated above, the concentration change of oxy- and deoxy-hemoglobin can be calculated from the variation in measured intensity of the back-scattered light at 735 and 850 nm respectively. The maximum output power of each wavelength is 30 mW, which is enough to ensure a high signal-to-noise ratio.

3.1.2 Detectors

Small detectors are preferred so that they can be embedded in the probe to directly detect back scattering photons exiting from the skin surface. Discrete photodiodes which are sensitive to near-infrared light can be used here. However, this kind of photocurrent detector is vulnerable to leakage current error. To minimize such errors, the following trans-impedance amplifier should be located as close as possible to the photodiode. As an integrated solution, a monolithic detector (OPT101, Texas Instruments, US) consisting of a photodiode and a trans-impedance amplifier is used. The detected signal is directly transduced into a voltage signal in the probe. OPT101 is the most sensitive in the wavelength range from 700 to 950 nm, and thus is well suited to near-infrared light detection. OPT101 is an 8-pin package and is small enough to be embedded in the probe. An external resistor is used to raise the voltage responsivity to a value of 3 V/μW. The bandwidth of OPT101 is set at 2.5 kHz, so that high frequency noise can be reduced and the frequency response is wide enough to satisfy the acquisition rate of 10 Hz.

3.1.3 Probe layout

For prefrontal cortex imaging, the probe is designed to cover the whole forehead of the subjects with a detection area of 15 cm × 4.4 cm.

The distance between the LED and the detector is determined by the depth to which penetration is required. In order to detect the signals from concentration changes of oxy- and deoxy-hemoglobin in the gray matter, the distance between each source and detector pair is set to be 2.89 cm. Monte Carlo simulation of a head model shows that, in this source-detector configuration, hemoglobin concentration changes from a depth of about 1.3 cm can be detected.

The probe consists of 4 LEDs as the light source and 10 detectors. As shown in Fig. 2, the LEDs and the detectors are arranged in an array and the detection area is divided into 16 sections (also called channels in the following text, each LED injects near-infrared light into the surrounding 4 sections), so that the functional activity can be mapped. When mounted on the forehead, signals from the fronto-polar prefrontal cortex, the dorsal lateral prefrontal cortex, and part of the ventral lateral prefrontal cortex can be detected.

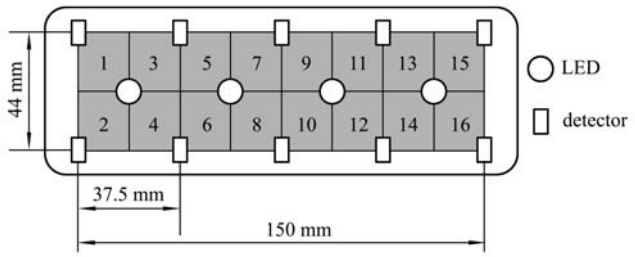

Fig. 2 Probe layout of functional imaging instrument

To ensure the flexibility of the probe so that it can be easily bent to fit to the forehead, a flexible printed circuit board (PCB) is used, to which the LEDs and detectors are soldered. The PCB is encapsulated in soft sponge. A piece of black sponge is used to cover the PCB surface except for the LEDs and detectors. The surface of the sponge is higher than the surface of the LEDs and the detectors by at least 0.1 cm, so it can exclude ambient light and prevent the near-infrared light from being picked up directly by the nearby detectors without propagating through the tissue.

3.2 Control box

3.2.1 LED driver module

The stability of the light source is very important in order to maximize accuracy. In order to maintain stability, a constant current LED driver (TB62726AN, Toshiba, Japan) is used. This chip has 16 output ports (each of which can be used to drive an LED) and 12 of them (4 LED each of 3 wavelength) are used in this system. The on and off of each LED is set via a serial interface consisting of a clock signal input and a serial data input. The two signals are provided by a USB data acquisition device. In order to minimize the cross talk between adjacent detection sections, the LEDs and different wavelengths in a single LED are turned on and off in sequence. The output current (the intensity of the LED) can be set using an external resistor.

3.2.2 Post-amplifier and low-pass filter

The output voltage signal from the probe has to be connected to the data acquisition device through a long cable. In order to increase input resistance to avoid distortion of the signal, a post-amplifier is used. The post-amplifier also raises the common-mode rejection ratio (CMRR) and provides a low output resistance to couple to the input of the data acquisition device. A Butterworth low-pass filter is used to suppress high frequency noise and electromagnetic interference from the surrounding environment.

3.3 Data acquisition device and software

To simplify the connection to the host PC, a USB data acquisition device (USB7310, ZTIC, China) is used and the host PC thus can be a laptop computer. The USB data acquisition device also provides the clock signal and the serial data to the LED driver and controls on and off of the LEDs. When one LED turns on, signals from the 4 detectors around it are acquired and digitized with 12 bit resolution by the USB device. After signals at different wavelengths have been acquired, the concentration

change of the hemoglobin in the surrounding four sections can be calculated. The shortest time needed for measurement on the whole 16 sections is about 100 ms.

The software was developed using Visual C++ 6.0. Timing requirement of LED drivers and signal acquisition process are coded in the software and the temporal resolution of this system can be adjusted from 100 to 1000 ms. Employing multithread programming technique, the software can also perform calculations and data curve plotting at the same time as the data is acquired. The calculation algorithm applied to the data is derived from Eqs. (3)–(5). The algorithm will automatically subtract the background signal (dark noise and stray light interference), which was detected ahead of each measurement cycle. The time course of the hemodynamic changes in the 16 detection sections can be displayed in real time and an activity map of the prefrontal cortex can be generated. Measurements can be saved in Excel or normal text format, and can be easily imported into other software, such as Matlab or SPSS, for further analysis. In order to facilitate the experiment, the software provides a programming interface and psychological stimulation pattern design can be easily integrated in.

4 Noise and long-term drift test

To evaluate system performances of the instrument, we measured the dark noise from the detectors and amplifiers. In this test, we put the probe in a black box to eliminate stray light and then displayed the signal output when all the light sources were turned off for half an hour. The results of this show that the noise level from the detectors and amplifiers ranges between 0.4 and 1.4 mV, which is comparable to 1 LSB output of the A/D converter in the USB device. In this test, we also find that the offset caused by the dark current is much larger than the noise level and is different from channel to channel. We use the background subtraction method to eliminate the offset in the software.

We also evaluated the stability performance of this instrument by a long-term drift test. Long-term drift was calculated by measuring the deviation of the initial and final voltage readings, when the probe was attached to a solid phantom for at least 1 hour. The drift is smaller than 0.7% in the one hour of monitoring. Hence, stability of the system is high enough for long-term experimentation.

5 Experiment and result analysis

In order to verify the ability of the instrument to monitor activity dependent hemodynamic processes, the Valsalva maneuver method is adopted [14,15]. Valsalva maneuver is used to evaluate the cardiovascular autonomic regulation and the regulation of cerebral blood flow velocity non-invasively. In this paper, the method was used to indirectly induce hemodynamic changes in the subjects' brain by changing the intrathoracic pressure. The hemodynamic change was monitored using the instrument.

The subject was a healthy 23-year-old male undergraduate student, who did not smoke, and never suffered from diabetes, neurological or cardiovascular diseases. The flexible probe was fixed on his forehead by an elastic bandage. The lower side of the probe and the subject's brow were at the same height and no hair covered the LEDs or the detectors. The subject was first asked to rest for 5 minutes. His blood pressure and pulse signals were recorded for 1 minute. After this, according to the requirement of the Valsalva maneuver, the subject was asked to take a breath as deep as possible to increase his intrathoracic pressure, then he was asked to hold his breath but still do the breathing action for 25 seconds and finally he was asked to breathe normally.

Hemodynamic changes during the Valsalva maneuver are calculated from the measurements and the time courses are plotted in Fig. 3. In Fig. 3, time courses of hemodynamic changes in channel 6 and channel 12 (see Fig. 2 for channel positions) are shown. The two vertical dashed lines represent the beginning and end of the Valsalva maneuver process. The characteristic behavior of different hemodynamic parameters during the process can be easily identified. The concentration change of HbO_2, compared with that of Hb shows larger increase at the beginning of the Valsalva maneuver and then gradually decrease as a consequence of continuous oxygen consumption.

Figure 4 shows the prefrontal cortical HbT and Hb concentration changes from the 16 channels of the instrument during the Valsalva maneuver process. The mean value and the standard deviation of the values from the 16 channels are shown in the plot. The two vertical bars represent the beginning and end of the Valsalva maneuver process. At the start of phase I, the arterial blood pressure increased instantaneously due to the increased pressure in the chest and abdominal cavity, CBF thus also increased rapidly. In phase II, the preload of the left ventricle and the blood pressure of the arteries decreased due to the decline of venous return, so CBF decreased too. The brain tissue continued to consume oxygen, so Hb concentration increased a little despite the decline in CBF. In phase III, the intrathoracic pressure was suddenly released, which caused the arterial pressure to decrease transiently. As a consequence, CBF fell significantly. In phase IV, CBF showed an overshoot and then returned gradually to the rest level.

The changes during the four phases of the Valsalva maneuver are consistent with previous physiological studies, which provide some validation of the instrument [15].

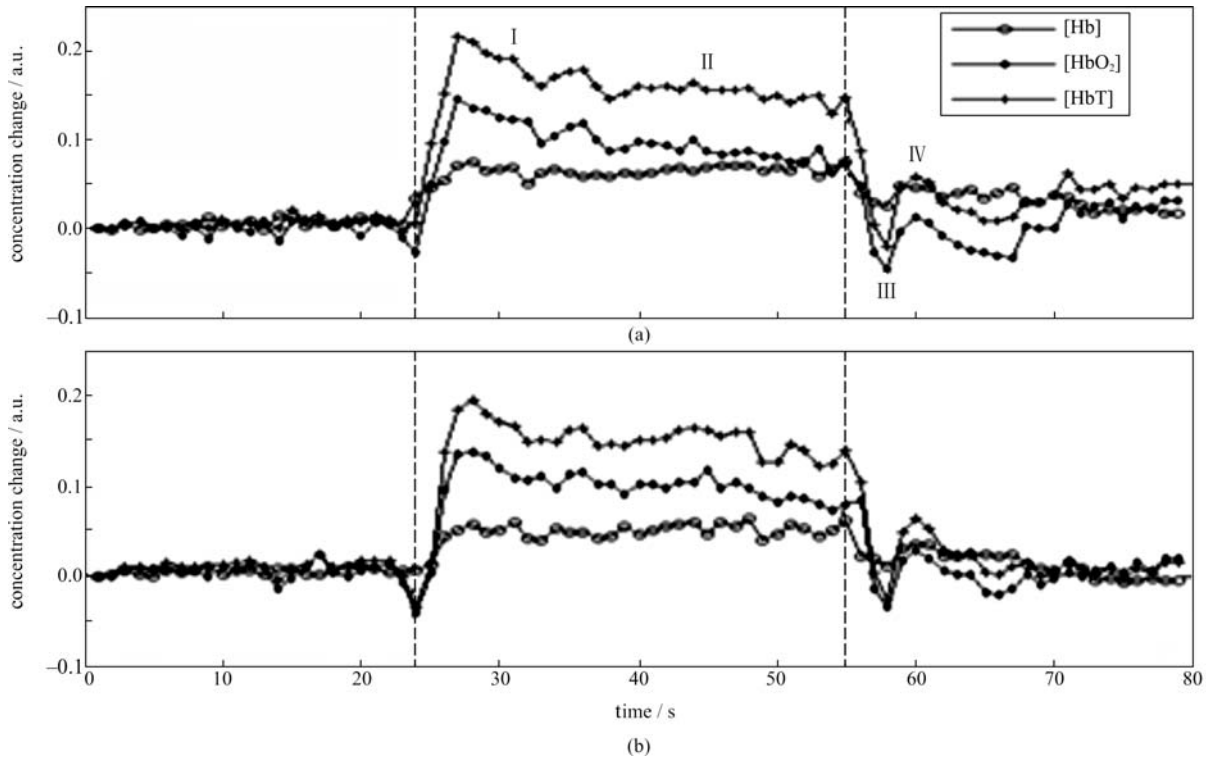

Fig. 3 Changes of [HbT], [HbO_2] and [Hb] at two channels during Valsalva maneuver. (a) Channel 6; (b) channel 12

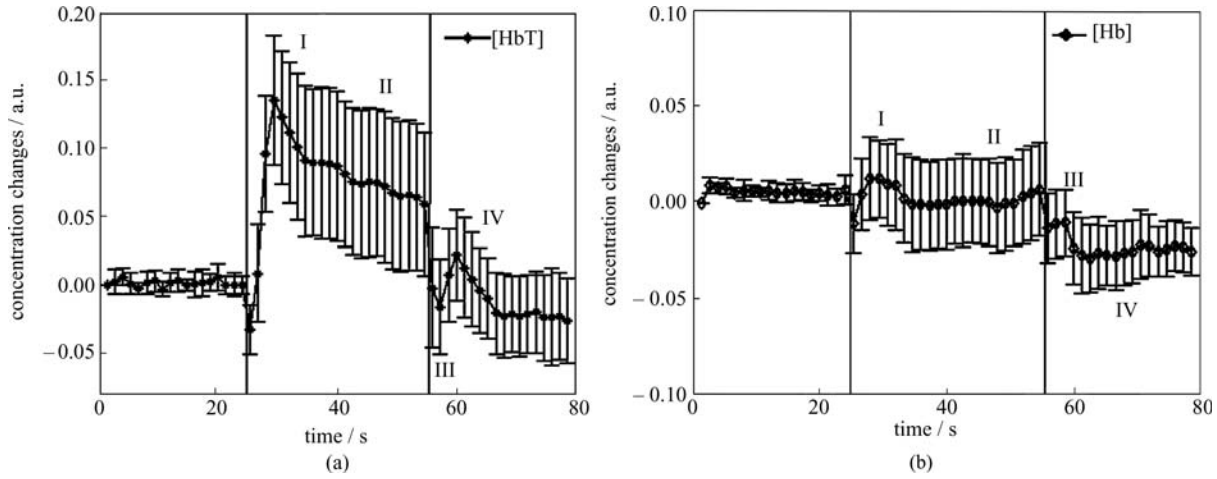

Fig. 4 [HbT] and [Hb] concentration changes during Valsalva maneuver. (a) Concentration change of [HbT]; (b) concentration change of [Hb]

6 Conclusion

In this paper, a functional imaging instrument based on NIRS that can be used to map functional activity in the prefrontal cortex is described and results of using it have been obtained. The results provide validation of the instrument. The probe is made of light-weight material and will not make the subjects feel uncomfortable. This feature and the portability of the instrument make it possible to conduct psychological experiments on the prefrontal cortex in a more natural way. Compared with other techniques, the instrument is much cheaper and easier to use and should be attractive to psychological researches that need a large number of experiments.

Acknowledgements This work was supported by the National Natural Science Foundation of China (Grant No. 30070261). The authors

would also like to give specific thanks to Professor William John Cram for reviewing the draft and commenting on English usages.

References

1. Steinmetz H, Furst G, Meyer B U. Craniocerebral topography within the international 10–20 system. Electroencephalography and Clinical Neurophysiology, 1989, 72(6): 499–506
2. Ogawa S, Lee T M, Kay A R, et al. Brain magnetic resonance imaging with contrast dependent on blood oxygenation. Proceedings of the National Academy of Sciences of the United States of America, 1990, 87(24): 9868–9872
3. Heeger D J, Ress D. What does fMRI tell us about neuronal activity. Nature Reviews Neuroscience, 2002, 3(2): 142–151
4. Villringer A, Chance B. Non-invasive optical spectroscopy and imaging of human brain function. Trends in Neurosciences, 1997, 20(10): 435–442
5. Franceschini M A, Fantini S, Thompson J H, et al. Hemodynamic evoked response of the sensorimotor cortex measured noninvasively with near-infrared optical imaging. Psychophysiology, 2003, 40(4): 548–560
6. Jöbsis F F. Noninvasive, infrared monitoring of cerebral and myocardial oxygen sufficiency and circulatory parameters. Science, 1977, 198(4323): 1264–1267
7. Hedden J C, Wong K S. Time-resolved optical tomography. Applied Optics, 1993, 32(4): 372–380
8. Chance B, Kang K A, He L, et al. Precision localization of hidden absorbers in body tissues with phased-array optical systems. Review of Scientific Instruments, 1996, 67(12): 4324–4332
9. Wariar R, Gaffke J N, Haller R G, et al. A modular NIRS system for clinical measurement of impaired skeletal muscle oxygenation. Journal of Applied Physiology, 2000, 88(1): 315–325
10. Metea M R, Newman E A. Glial cells dilate and constrict blood vessels: a mechanism of neurovascular coupling. The Journal of Neuroscience, 2006, 26(11): 2862–2870
11. Hazeki O, Tamura M. Quantitative analysis of hemoglobin oxygenation state of rat brain in situ by near-infrared spectrophotometry. Journal of Applied Physiology, 1988, 64(2): 796–802
12. Shiga T, Yamamoto K, Tanabe K, et al. Study of an algorithm based on model experiments and diffusion theory for a portable tissue oximeter. Journal of Biomedical Optics, 1997, 2(2): 154–161
13. Lin Y, Lech G, Nioka S, et al. Noninvasive, low-noise, fast imaging of blood volume and deoxygenation changes in muscles using light-emitting diode continuous-wave imager. Review of Scientific Instruments, 2002, 73(8): 3065–3074
14. Wang Qiang, Zhang Zhengguo, Luo Zhicheng. Noninvasive assessment of the dynamic cerebrovascular regulation. Chinese Journal of Biomedical Engineering, 2002, 21(6): 563–567 (in Chinese)
15. Tiecks F P, Douville C, Byrd S, et al. Evaluation of impaired cerebral autoregulation by the Valsalva maneuver. Stroke, 1996, 27(7): 1177–1182